

Statistical modeling and CMIP5 simulations of hot spell changes in China

Weiwen Wang · Wen Zhou · Yun Li · Xin Wang ·
Dongxiao Wang

Received: 23 January 2014 / Accepted: 5 August 2014 / Published online: 19 August 2014
© Springer-Verlag Berlin Heidelberg 2014

Abstract A hot spell is an extreme weather event with one or more consecutive days with daily maximum temperature exceeding a certain threshold of high temperature. Statistical modeling of summer hot spells in China during 1960–2005 and their simulations in the historical experiment of the Coupled Model Intercomparison Project Phase 5 (CMIP5) are investigated in this study. A technique called the hot spell model (HSM), introduced by Furrer et al. (Clim Res 43:191–205, 2010) for modeling hot spells by extending the point process approach to extreme value theory, is applied. Specifically, the frequency of summer hot spells is modeled by a Poisson distribution, their intensity is modeled by a generalized Pareto distribution, and their duration is modeled by a geometric distribution. Results show that the HSM permits realistic modeling of summer hot spells in China. Trends in the frequency, duration, and intensity of hot spells were estimated based on the HSM for the observed period from 1960 to 2005. Furthermore, the performance in simulating hot spell characteristics and trends from the CMIP5 historical run were assessed based on the HSM. Climate models with good performance were selected to conduct an ensemble projection of hot spell

intensity, frequency, and duration and their trends in future decades.

Keywords Hot spell model · Extreme value theory · CMIP5

1 Introduction

Extreme hot events in summertime, such as hot spells and heat waves with sustained high temperatures, have been known to produce notable effects on human mortality, regional economies, and ecosystems, and these impacts are increasing under the background of global warming (e.g., Easterling et al. 2000; Parmesan et al. 2000; Meehl and Tebaldi 2004). To assess past changes in hot extremes as well as possible future consequences, an adequate definition of hot extremes is important (Robinson 2001). Different definitions have been applied to quantify the frequency, intensity, and duration of this extreme weather event (e.g., Jones et al. 1999; Karl et al. 1999). Generally, a hot day is defined as a day in which the daily maximum temperature (T_{\max}) exceeds a certain threshold of high temperature. A hot spell is defined as one or more (consecutive) hot days. A heat wave can be indirectly derived from hot spells, such as longer hot spells or clustered shorter hot spells (Furrer et al. 2010). Furthermore, variable spatial scales may be involved in the identification of heat waves. The thresholds used in the definitions of the above extreme events can be either absolute (e.g., 35 °C in China) or relative (e.g., 95th percentile of daily T_{\max}) (Yan et al. 2002). In this study, we focus on summer hot spells with a relative threshold.

China has experienced remarkable changes in summer heat extremes during recent decades (Ding and Qian 2011; Gong et al. 2004; Qian and Lin 2004; Qian et al. 2011a; Su

W. Wang · W. Zhou (✉)
Guy Carpenter Asia-Pacific Climate Impact Centre, School
of Energy and Environment, City University of Hong Kong,
Hong Kong 00852, China
e-mail: wenzhou@cityu.edu.hk

Y. Li
CSIRO Computational Informatics, Wembley, WA 6913,
Australia

X. Wang · D. Wang
State Key Laboratory of Tropical Oceanography, South China
Sea Institute of Oceanology, Chinese Academy of Sciences,
Guangzhou, China

et al. 2006; Yan et al. 2011; You et al. 2008). Previous studies have suggested these changes but there has been uncertainty about the exact patterns in different areas of China. For example, Zhai and Pan (2003) noted that the number of hot days displayed a slightly decreasing trend, while increasing trends were detected in the frequencies of warm days and warm nights for China as a whole during 1951–1999. Zhang et al. (2008) found a significant upward trend in both the frequency and intensity of summer extreme high temperature events in the western and northern regions of the Yellow River basin, while trends in eastern China were mainly not significant.

There is a long tradition of using extreme value distributions in environmental applications. In early studies, the generalized extreme value (GEV) distribution with unchanged parameters was applied in order to model simple climatic extreme events, usually in the form of block maxima, such as annual maxima of daily precipitation or temperature (Gumbel 1958). Such studies typically assumed stationarity, that is, an unchanging climate. However, this assumption has become untenable with our currently changing climate (e.g., Qian et al. 2011b).

Later, attempts were made to surmount these shortcomings. On the one hand, the theory has been extended to encompass temporal trends. The most common approach for dealing with nonstationarity is to allow for parametric changes with time in the GEV distribution. Linear trends in GEV parameters are a first step and have shown practical utility in assessing long-term changes in climatic extremes. On the other hand, the peaks-over-threshold model has been used to describe all exceedances above a high threshold instead of just looking at block maxima (e.g., Todorovic and Zelenhasic 1970). The so-called point process approach was hence proposed (e.g., Smith 1989). This method jointly models the occurrence of an event (an exceedance of a high threshold) and its severity (the degree of excess over a high threshold). The exceedances are assumed to occur according to a Poisson distribution, while the excesses above the threshold are assumed to follow a generalized Pareto (GP) distribution (e.g., Coles 2001).

Statistical modeling of extreme values has been widely used in studies of meteorological and hydrological extremes in recent decades under the background of rapid climate change (e.g., Furrer and Katz 2008; Katz et al. 2002, 2005; Li et al. 2005; Meehl et al. 2000). In the statistical modeling studies of hot spells, it is common to decluster the data and model only frequency and severity (e.g., Brown et al. 2008; Nogaj et al. 2006; Zhang et al. 2004). Furrer et al. (2010) advocated an approach to modeling hot spell length using the temporal dependence of excesses within a hot spell, rather than discarding these clusters. This approach is adopted in this study and applied to hot spell modeling in China, where statistical modeling

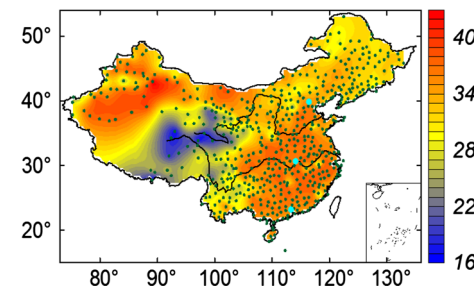


Fig. 1 Observational thresholds (*color shading*) in China. *Small green dots* denote the 549 gauge stations. The three *larger blue dots* indicate the three demonstration stations at Beijing, Wuhan, and Guangzhou, respectively, from north to south

of hot spells based on extreme value theory has rarely been applied in previous studies. In addition, these statistical methods are applied to data from the Coupled Model Intercomparison Project Phase 5 (CMIP5) (Taylor et al. 2012) to assess simulations of hot spells over China in these state-of-the-art climate models.

The data used in this study and the statistical modeling method for hot spells are described in the next section. The results of the statistical modeling of hot spells in terms of frequency, intensity, and duration (length) are presented in Sect. 3, while an assessment of CMIP5 simulations with future projections of hot spell components is given in Sect. 4. The final section summarizes and discusses our main findings.

2 Data and methodology

2.1 Data

Homogenization of observation data is important for climatic extreme studies. A homogenized historical temperature dataset for China (Li and Yan 2009) includes a homogenized daily maximum temperature series from 549 stations in China spanning from 1960 to 2008. The geographic distribution of the stations is shown in Fig. 1. The stations are evenly distributed in the plains of East China, but scarce on the Tibetan Plateau and in the Tarim Basin in Northwest China. This homogenized dataset has been widely used in temperature extreme studies in recent years (e.g., Wang et al. 2013a, 2014; Yan et al. 2011). T_{\max} is used to define hot extremes in this study. Note that observation data from 1960 to 2005 are used, as the main run of the CMIP5 historical simulations ends in 2005.

The CMIP5, in support of the 5th assessment report (AR5) of the Intergovernmental Panel on Climate Change (IPCC), provides simulations from a new generation of global climate models (GCMs) (IPCC 2013). The 30

Table 1 List of CMIP5 GCMs used in this study, with horizontal resolutions given in the form of global numbers of meridional and zonal levels, and uncentered pattern correlation coefficients of hot spell trends between GCMs and observations

No.	Acronyms	Resolution (lat × lon)	Intensity trend	Frequency trend	Length trend
1	ACCESS1-0	145 × 192	0.04	0.15*	-0.09
2	ACCESS1-3	145 × 192	-0.05	0.13*	0.04
3	BCC-CSM1-1	64 × 128	0.06	0.18*	-0.00
4	BCC-CSM1-1-m	160 × 320	0.04	0.24*	0.23*
5	BNU-ESM	64 × 128	-0.04	0.17*	0.28*
6	CanESM2	64 × 128	0.22*	0.29*	0.41*
7	CCSM4	192 × 288	0.01	0.23*	0.34*
8	CESM1-BGC	192 × 288	0.02	0.15*	0.27*
9	CESM1-CAM5	192 × 288	0.18*	0.24*	0.27*
10	CMCC-CM	240 × 480	0.15*	0.15*	0.08*
11	CMCC-CMS	96 × 192	0.10*	0.28*	0.27*
12	CNRM-CM5	128 × 256	0.06	0.25*	0.16*
13	CSIRO-Mk3-6-0	96 × 192	-0.08	-0.06	0.02
14	FGOALS-g2	60 × 128	0.10*	0.15*	0.46*
15	GFDL-CM3	90 × 144	0.26*	0.25*	0.32*
16	GFDL-ESM2G	90 × 144	-0.00	0.22*	0.16*
17	GFDL-ESM2 M	90 × 144	0.28*	0.15*	0.43*
18	HadGEM2-CC	145 × 192	0.08*	0.03	0.39*
19	HadGEM2-ES	145 × 192	0.14*	-0.04	0.25*
20	INM-CM4	120 × 180	-0.09	0.15*	0.06
21	IPSL-CM5A-LR	143 × 144	0.05	0.24*	0.26*
22	IPSL-CM5A-MR	143 × 144	0.05	0.24*	0.26*
23	IPSL-CM5B-LR	96 × 96	0.17*	0.24*	0.47*
24	MIROC5	128 × 256	0.17*	0.12*	0.08*
25	MIROC-ESM	64 × 128	-0.06	-0.12	-0.26
26	MIROC-ESM- CHEM	64 × 128	0.08*	-0.04	0.07
27	MPI-ESM-LR	96 × 192	0.17*	0.24*	0.34*
28	MPI-ESM-MR	96 × 192	0.11*	0.27*	0.30*
29	MRI-CGCM3	160 × 320	0.03	0.12*	0.39*
30	NorESM1-M	96 × 144	0.10*	0.24*	0.33*

* Significant positive correlation coefficient at the 0.05 level

GCMs used in the present study are listed in Table 1, along with their horizontal resolutions. Vertical resolutions are not shown, as only near-surface T_{\max} is used in this study. The historical experiment and two “representative concentration pathway” (RCP) scenarios, RCP4.5 and RCP8.5, are involved. See Taylor et al. (2012) for details on the CMIP5 experimental design. The time periods for the historical and RCP experiments used in this study are 1960–2005 and 2006–2100, respectively. For convenience of comparison with observations, all T_{\max} data from the GCMs are interpolated to the locations of the gauge stations in space using a two-dimensional linear interpolation.

2.2 Definition of a hot spell

To express the “extreme” character of a hot spell, appropriate thresholds are needed. Appropriate thresholds are also necessary for fitting the point process model. In this study, the 95th percentile of summer (June–July–August, JJA) T_{\max} at each station during the base period of 1961–1990 is adopted as the hot spell threshold, which can simply be expressed as “extreme.” Different base periods will result in different mean annual cycles and anomalies in a changing climate (Qian et al. 2011b). The base period of 1961–1990 is chosen in reference to the Expert Team for Climate Change Detection Monitoring and Indices (ETC-CDMI). The selected thresholds based on the 95th percentile of JJA T_{\max} are shown in Fig. 1 (the shadings). A hot day is defined as a day when the T_{\max} is higher than this threshold. A hot spell is an extreme hot event with one or more consecutive hot days. The number of days a hot spell persists is defined as its duration, and the maximum T_{\max} within a hot spell is defined as its intensity. Hot spell frequency is the number of occurrences in one summer.

2.3 Bias correction of climate model data

Climate models are not perfect in simulating the climate. There is a difference between simulated and observed variables, which is known as bias. Generally, the bias in air temperature simulated by GCMs can be as much as a few degrees Celsius. To obtain more accurate future projections and make them applicable to impact studies, it is crucial to remove this bias from model outputs. A bias correction procedure is therefore performed in this study:

$$T = T_{GCM} - (U_{GCM} - U_{OBS}) \quad (1)$$

where U_{GCM} is the 95th percentile threshold in climate models, U_{OBS} is the threshold of observations (i.e., the shading in Fig. 1), T_{GCM} is the T_{\max} output of the climate model in each location (interpolated to 549 observational sites), and T is the T_{\max} data with bias corrected and will be used in hot spell calculations. This procedure is applied to each GCM in each location, so that biases are systematically reduced. In calculating the hot spells following this correction, U_{OBS} is adopted in all GCMs. In practice, this correction will affect only the magnitudes of hot spell intensity, not frequency or duration.

2.4 Statistical model

We applied the hot spell model (HSM) introduced by Furrer et al. (2010) to study hot spells. The HSM extends the point process approach to extreme value theory to model the frequency, duration, and intensity of hot spells. Specifically, the annual frequency of hot spells is modeled by a

Poisson distribution, their intensity is modeled by a generalized Pareto (GP) distribution, and their duration is modeled by a geometric distribution.

Accordingly, assuming that the threshold (i.e., the 95th percentile of summer T_{\max}) is appropriate to define a hot spell event, the number of occurrences (frequency) of hot spells can be modeled by a Poisson distribution with rate λ . The probability mass function of the Poisson distribution is given by

$$P(k) = \frac{\lambda^k e^{-\lambda}}{k!}, \quad k = 1, 2, \dots \quad (2)$$

The intensity (the maximum excess within a hot spell) can be approximately fitted to a GP distribution given by

$$F(x; \xi, \sigma_u, u) = 1 - \left[1 + \xi \frac{x - u}{\sigma_u} \right]^{-\frac{1}{\xi}}, \quad (3)$$

$$x > u, \quad 1 + \xi \frac{x - u}{\sigma_u} > 0$$

where ξ stands for the shape parameter, $\sigma_u > 0$ denotes the scale parameters depending on the selected threshold u , and $-\infty < \mu < \infty$ is the location parameter. For temperature, negative shape parameters, that is, those with a bounded tail, are supposed to be obtained (e.g., Brown and Katz 1995).

The length (duration) of hot spells may be modeled with a geometric distribution given by

$$P(k) = (1 - \theta)^{k-1} \theta, \quad k = 1, 2, \dots \quad (4)$$

with the reciprocal of the parameter θ being the mean. Parameter estimation in the HSM [i.e., Eqs. (2)–(4)] is done using maximum likelihood methods.

The HSM is further extended to allow for estimate trends in hot spell frequency, intensity, and duration characteristics. For all three model components, one can consider parameters fixed over the summer season within a given year but allow shifts from 1 year to another. That is, for each year x in the record period, $\lambda = \lambda(x)$ for the Poisson parameter, $\sigma_u = \sigma_u(x)$ for the GP scale parameter, and $\theta = \theta(x)$ for the geometric parameter. Since changes in the shape parameter of the GP distribution are rarely observed and difficult to model, this parameter is kept fixed. Trends are introduced through a generalized linear model (GLM) framework in the Poisson and the geometric model and through covariate effects in the GP scale parameter. See more details in Furrer et al. (2010).

2.5 Pattern correlation

The uncentered pattern correlation coefficient is used to evaluate the performance of the GCMs in simulating hot spell trends. The pattern correlation is a Pearson linear

correlation, particularly in this study, between the same parameter (e.g., trend of hot spell frequency) in corresponding locations of the map in observations and GCMs. Pattern correlation can be either centered (Santer et al. 1993) or uncentered (Barnett and Schlesinger 1987). The centered (uncentered) correlation correlates two fields with (without) the removal of global means. It has been argued that the uncentered pattern correlation is better suited for climate change detection (IPCC 2001; Legates and Davis 1997). In this study, the uncentered pattern correlation is calculated by:

$$C = \frac{\sum_{i=1}^n x_i y_i}{\sqrt{\sum_{i=1}^n x_i^2} \sqrt{\sum_{i=1}^n y_i^2}} \quad (5)$$

where x and y are the parameters in observations and GCMs, respectively, with the same size spatial point n .

3 Hot spells in observation records

To clearly elucidate the application of the HSM and its performance in fitting the observational records, three cases for gauge stations in eastern China, where there is a high population density and more economic activity (e.g., Gong et al. 2004), are presented here. These sample locations, from north to south, are Beijing, Wuhan, and Guangzhou, as shown in Fig. 1, and are representative cities of northern, east-central, and southern China, respectively. As the capital city of China, Beijing has received more attention in extreme climate studies, including site change and urbanization (Yan et al. 2010), homogenization of daily temperature series (Li and Yan 2010), and extreme temperature trends (Yan et al. 2001), compared to other sites in China. Summer high temperature extremes are found to occur with high frequency in the eastern Yangtze River Valley (e.g., Su et al. 2006). Wuhan is one of the well-known hot cities in this region and has been taken as a representative station together with Beijing in a previous study (Ren et al. 2007). Finally, Guangzhou is chosen to represent southern China, particularly the Pearl River Basin, where there is a fast-growing population and industrialization; Guangzhou was also investigated in a recent climate extreme study (Fischer et al. 2013).

The threshold is 35.0 °C for Beijing, 36.9 °C for Wuhan, and 35.5 °C for Guangzhou, as listed in Table 2. Estimated parameters with standard errors in parentheses of the GP, Poisson, and geometric distributions of hot spells at these sites are also listed in Table 2. Figure 2 suggests that based on these fitted distributions, the HSM permits realistic modeling of summer hot spells at these illustrative sites. We obtained a scale parameter for the GP distribution (σ_u) of 1.65 for Beijing, 1.15 for Wuhan, and 1.14 for Guangzhou.

Table 2 Selected thresholds and estimated parameters (standard errors in parentheses) of GP, Poisson, and geometric distributions of hot spells in Beijing, Wuhan, and Guangzhou

	Beijing	Wuhan	Guangzhou
Threshold (°C)	35.0	36.9	35.5
GP Scale (σ_u)	1.65 (0.195)	1.15 (0.138)	1.14 (0.147)
Poisson (λ)	3.48 (0.539)	2.00 (0.388)	3.72 (0.557)
Geometric (θ)	0.57 (0.045)	0.43 (0.052)	0.60 (0.045)

The thresholds are calculated for a climatological base period of 1961–1990, while the fitting parameters are estimated in the study period of 1960–2005

Based on these estimations and fitting, histograms for the clustered maximum excesses under the GP hypothesis are shown in the top panels of Fig. 2. All the quantile–quantile plots (not shown) suggest that there is no major deviation between the empirical and fitted distributions. The mean hot spell intensity for Beijing, Wuhan, and Guangzhou is 36.5, 37.7, and 36.4 °C, respectively.

We obtained a Poisson parameter (λ) of 3.48, 2.00, and 3.72 for Beijing, Wuhan, and Guangzhou, respectively. The middle panels in Fig. 2 show the number of clusters per summer in observations, denoted in circles, along with the estimated Poisson probability distribution function (PDF), expressed by the line. Although there are discrepancies, observations are generally in accord with the fitted distribution.

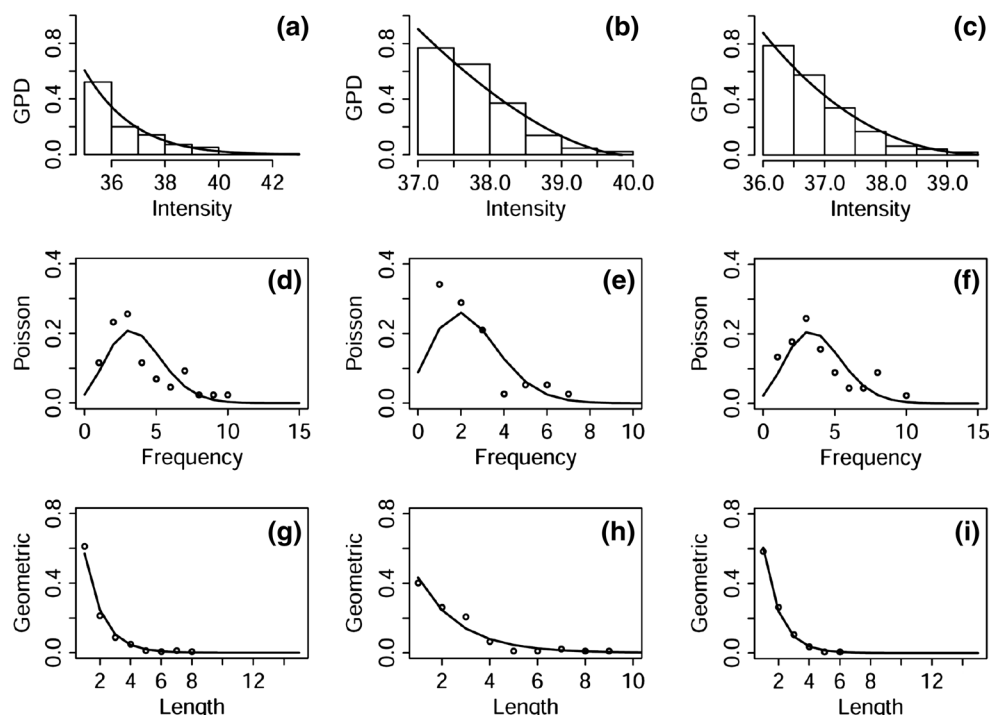
Estimated parameters of the geometric distribution (θ) for hot spell duration are given in Table 2. The mean hot

spell duration ($1/\theta$) for Beijing, Wuhan, and Guangzhou is 1.75, 2.32, and 1.67 days, respectively. Observed (circles) hot spell durations along with the estimated geometric PDF (line) of the three illustrative sites are shown in the lower panels of Fig. 2. These graphs demonstrate the good agreement between the observations and HSM predictions.

The following discussion of hot spell trend estimation is based on the above fitting methodology. The frequency (number of hot spell occurrences in one summer) and duration are obtained from the hot spell definition, while the intensity can be measured by the mean, maximum, or total excess of one hot spell. Here we use the maximum excess. This indicator can be better fitted in the HSM when T_{max} has a small fluctuation, for example, <1 °C in a hot spell. Finally, trends in all three characteristics can be calculated when we fix parameters within a given summer but allow changes from 1 year to another, as introduced in the methodology of the statistical model.

Estimated trends in hot spell intensity, frequency, and duration at the three illustrative sites are shown in Fig. 3. Interannual and interdecadal variations in these hot spell characteristics can be seen in these diagrams (the stems), but here we focus only on their trends, which are denoted by the thick lines. Estimated trends at the three sites are given in Table 3. p Values of the log-likelihood test are also computed (values in parentheses in Table 3), which express the significance level of trends estimated by the HSM. It is found that the trends of duration in Beijing, the intensity in Wuhan, and the frequency and duration in Guangzhou are significant at the 0.05 level. We further demonstrate the

Fig. 2 Fitting intensity (a–c, °C), frequency (d–f, events/year), and length (duration) (g–i, days) of summer hot spells to GP, Poisson, and geometric distributions in Beijing (a, d, g), Wuhan (b, e, h), and Guangzhou (c, f, i)



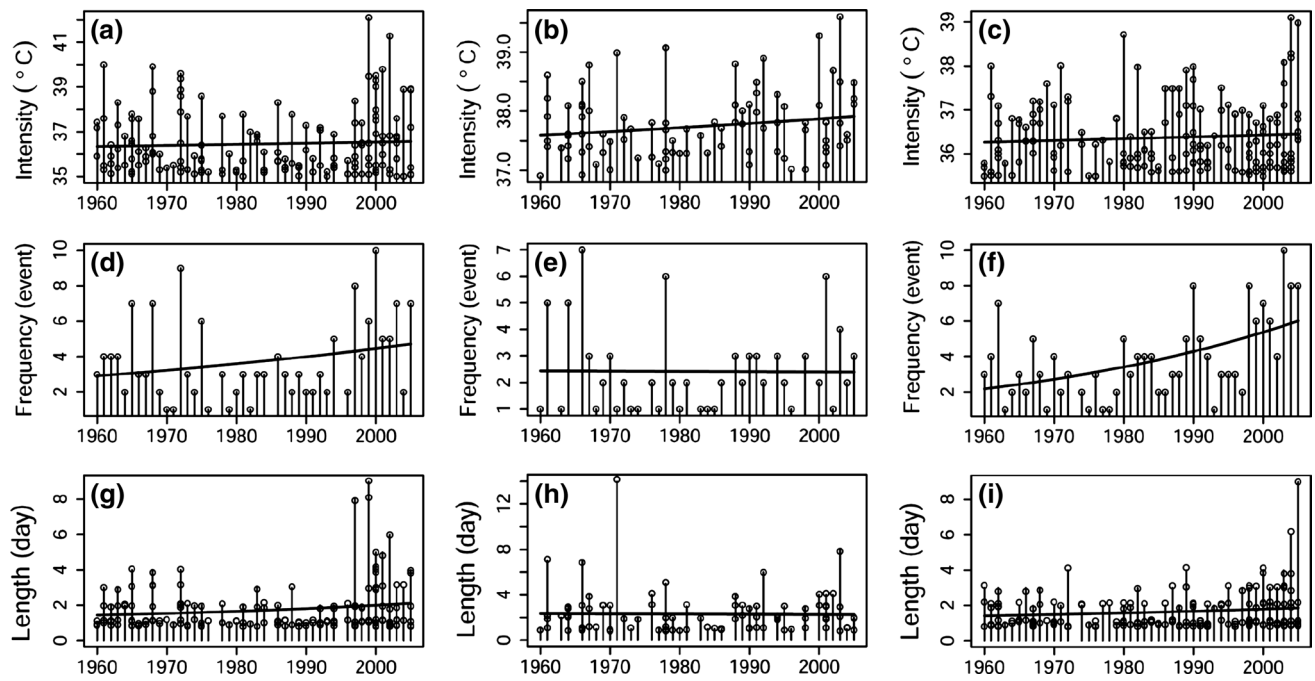


Fig. 3 Trends of hot spell intensity (**a–c**, °C/year), frequency (**d–f**, events/year), and length (**g–i**, days/year) in Beijing (**a, d, g**), Wuhan (**b, e, h**), and Guangzhou (**c, f, i**) during 1960–2005 estimated by the HSM

Table 3 Estimated trends (*p* values in parentheses) of hot spell frequency, duration, and intensity in Beijing, Wuhan, and Guangzhou in 1960–2005

	Beijing	Wuhan	Guangzhou
Intensity (°C/year)	0.004 (0.39)	0.008 (0.03)	0.003 (0.53)
Frequency (events/year)	0.011 (0.07)	0.000 (0.96)	0.023 (0.00)
Duration (days/year)	0.021 (0.02)	-0.001 (0.89)	0.017 (0.04)

HSM estimate trends in hot spell components by taking the hot spell frequency in Guangzhou (Fig. 3f) as an example. The trend in the number of hot spells is estimated based on a fitted non-stationary Poisson distribution with the parameter rate changing with the year (x): $\lambda(x) = \exp(\beta_0 + \beta_1 x)$. The GLM framework is used to estimate the parameters. Specifically, for the number of hot spells in Guangzhou, the trend is estimated by $\exp(-45.53 + 0.023x)$. That is, the number of hot spells increases exponentially at the rate of 0.023 event/year, which is significant at the 0.05 level (Table 3). Using simple linear regression to estimate the trend in the number of hot spells is not recommended based on two concerns: first, the trend estimation based on the linear model assumes the data follow a normal distribution, which is not realistic for modeling extreme events; second, the linear trend fails to capture the nonlinear behavior in the number of hot spells. For the example of hot spell frequency in Guangzhou, the linear trend can be estimated by

$162.53 + 0.084x$, with a slope of 0.084 event/year, which does indeed fail to capture the nonlinear trend in the number of hot spells.

Hot spells at all 549 gauge stations in China are modeled using the HSM. The climatological mean of summer hot spell intensity estimated by the HSM is shown in Fig. 4a. The spatial patterns of the intensity are close to the threshold in Fig. 1, and they both resemble the climatological temperature pattern of China. Note that the colored bars of Figs. 1 and 4a are the same. The threshold varies from 16.6 to 42.3 °C, while the mean hot spell intensity is about 1 °C higher, with a range of 17.4–43.4 °C.

The relative definition of hot spells using percentile thresholds leads to a reversed geographic pattern of hot spell frequency and duration (Fig. 4b, c). In addition, hot spells in the lower Yangtze River valley persist longer than those in other areas of China (Fig. 4c). The reasons for this may relate to the maintenance of the western North Pacific subtropical high and the emergence of a rain belt in east-central China (Tao and Wei 2006). Furthermore, hot spells with higher frequencies and shorter durations are found in southwestern and northeastern China. Finally, for China as a whole, the hot spell frequency is around 1.7–3.8 events/summer while the mean duration is around 1.3–3.1 days.

Estimated trends of three characteristics of hot spells in China are shown in Fig. 4d–f. Only trends that are significant at the 0.05 level are plotted, that is, *p* values <0.05 for the likelihood ratio test for the null hypothesis that

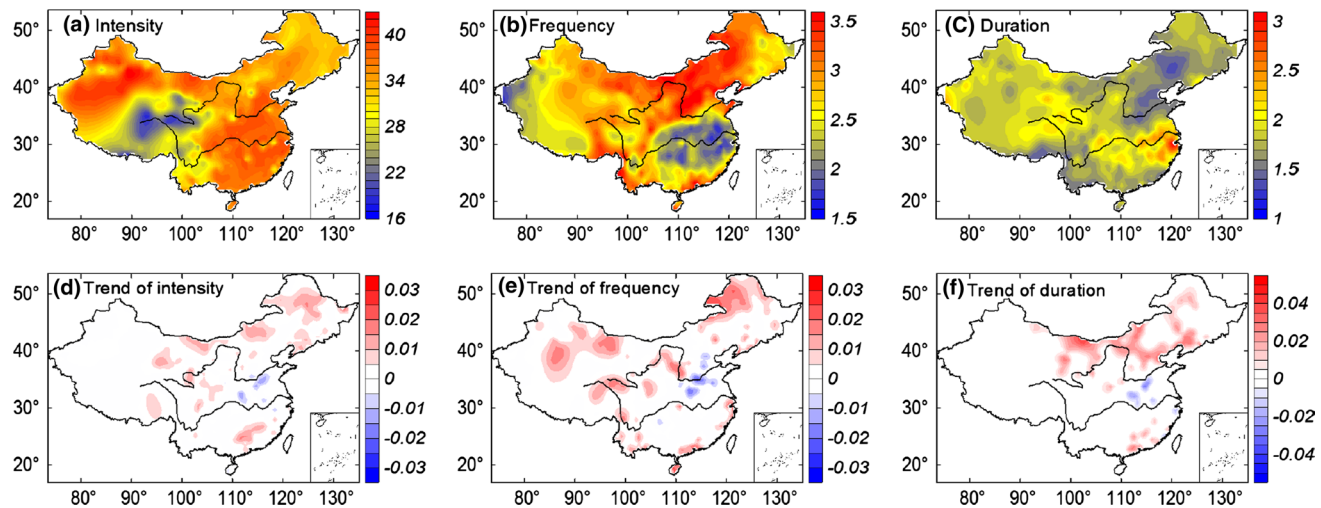


Fig. 4 Geographic distributions of estimated intensity (a, $^{\circ}\text{C}$), frequency (b, events/year), duration (c, days), trends in intensity (d, $^{\circ}\text{C}/\text{year}$), trends in frequency (e, events/year), and trends in duration (f, days/year)

based on the HSM using observed daily maximum temperature data from 1960 to 2005. Only trends significant at the 0.05 level are plotted

there is no trend in the fitted models. Trends are -0.013 to 0.016 $^{\circ}\text{C}/\text{year}$, -0.026 to 0.025 events/year, and -0.030 to 0.038 days/year for intensity, frequency, and duration, respectively. Overall, significant trends are localized for all three hot spell components. Significant increasing trends are widespread in northern China and some coastal regions in Southeast China. It is noteworthy that significant decreasing trends in all three hot spell components are found in a small region of east-central China. Decreasing trends in summer high temperatures in this region are also evident in previous studies (e.g., Figure a3 in Qian et al. 2011a). Previous studies have suggested natural and anthropogenic forcing as possible reasons for this regional summer surface cooling. For natural forcing, it was found that the cooling downstream of the Tibetan Plateau is associated with the weakening of the East Asian summer monsoon and the southward displacement of the upper-level westerly jet stream (Ding et al. 2009; Wang et al. 2013b; Yu et al. 2004; Yu and Zhou 2007; Zhou et al. 2006). Recent studies further revealed that this summer monsoon weakening is related to sea surface temperature forcing and the Pacific decadal oscillation (Li et al. 2010; Qian and Zhou 2014). For anthropogenic forcing, human-made aerosols may have played an important role in this regional climate change (Li et al. 2007; Menon et al. 2002; Ueda et al. 2006; Xu 2001).

4 CMIP5 simulations

GCMs in CMIP5 are generally based on more comprehensive Earth climate systems and have a higher spatial resolution compared to the previous generation (CMIP3), hence

lending more confidence to climatic extreme studies, which is one of the important tasks in IPCC AR5. CMIP5 studies have looked at robustness and uncertainty (Knutti and Sedlacek 2012), surface temperature (Jones et al. 2013), and climate extremes (Sillmann et al. 2013a, b) and have recently been subjects of widespread discussion. As a follow-up study on the observed hot spells based on the HSM, CMIP5-simulated hot spells in China are investigated in this section, including evaluation of historical experiments and projection of future RCP scenarios.

4.1 Historical simulations

Thirty GCMs listed in Table 1 are basically all the GCMs in CMIP5 for which T_{\max} in both the historical experiment and future scenarios (RCP4.5 and RCP8.5 spanning from 2006 to 2100) are available. First of all, the performances of these climate models on their simulation of hot spell characteristics are evaluated. GCMs with good performance will be selected in the future projection to estimate the trend in hot spell components in the upcoming decades of this century in China. With this objective in mind, the main criterion of “good performance” is that the geographic pattern of trends in the historical experiment can reproduce good similarity with the observations.

The HSM is applied to all historical runs of the 30 GCMs. Trends of all three hot spell components over China are obtained and their uncentered pattern correlation coefficients with observations (Fig. 4d-f) are computed. These correlation coefficients are listed in Table 1 to quantify the similarity. It is noteworthy that these correlation coefficients are calculated with nonsignificant trends (p value larger than 0.05) in the observation set to zero, as we focus

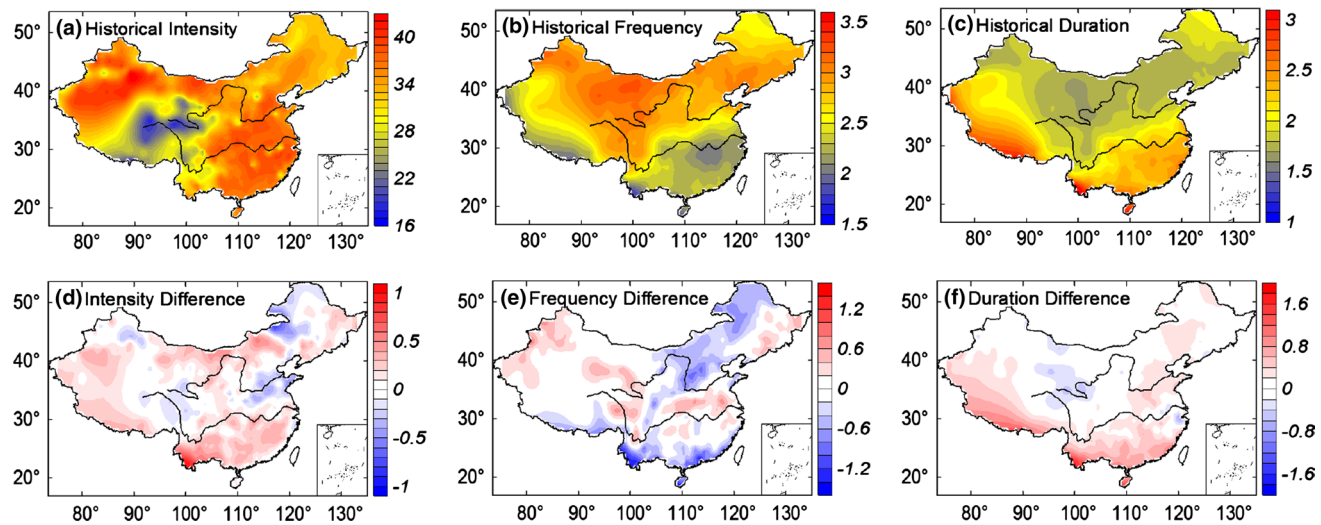


Fig. 5 Ensemble mean of hot spell intensity (**a**, °C), frequency (**b**, events/year), and duration (**c**, days) of 12 GCMs in the historical run, and the intensity difference (**d**, °C), frequency difference (**e**, events/

year), and duration difference (**f**, days) between the ensemble mean and observations in 1960–2005

only on the spatial pattern of significant trends. As the total sample number is 549 (number of stations), the degrees of freedom are simply estimated at 547. Therefore, a correlation coefficient of 0.08 or above is significant at the 0.05 level. It is found that only 50 % (15 out of 30) GCMs can obtain a significant positive pattern correlation with observed trends in hot spell intensity, while about 83.3 % (25 out of 30) GCMs can get a significant positive pattern correlation with observed trends in hot spell frequency. The percentage of GCMs that shows significant pattern correlation with observed trends in hot spell duration is 23 out of 30, that is, 76.7 % approximately. Based on Table 1, we selected 12 GCMs that have significant positive pattern correlation with observed trends in all three hot spell components. These GCMs are CanESM2, CESM1-CAM5, CMCC-CM, CMCC-CMS, FGOALS-g2, GFDL-CM3, GFDL-ESM2M, IPSL-CM5B-LR, MIROC5, MPI-ESM-LR, MPI-ESM-MR, and NorESM1-M. Practically, we have to point out that the performance of climate models involves many aspects. It is hard to say which GCM is good and which is not. The criterion we use here is just a relative one, considering our objective.

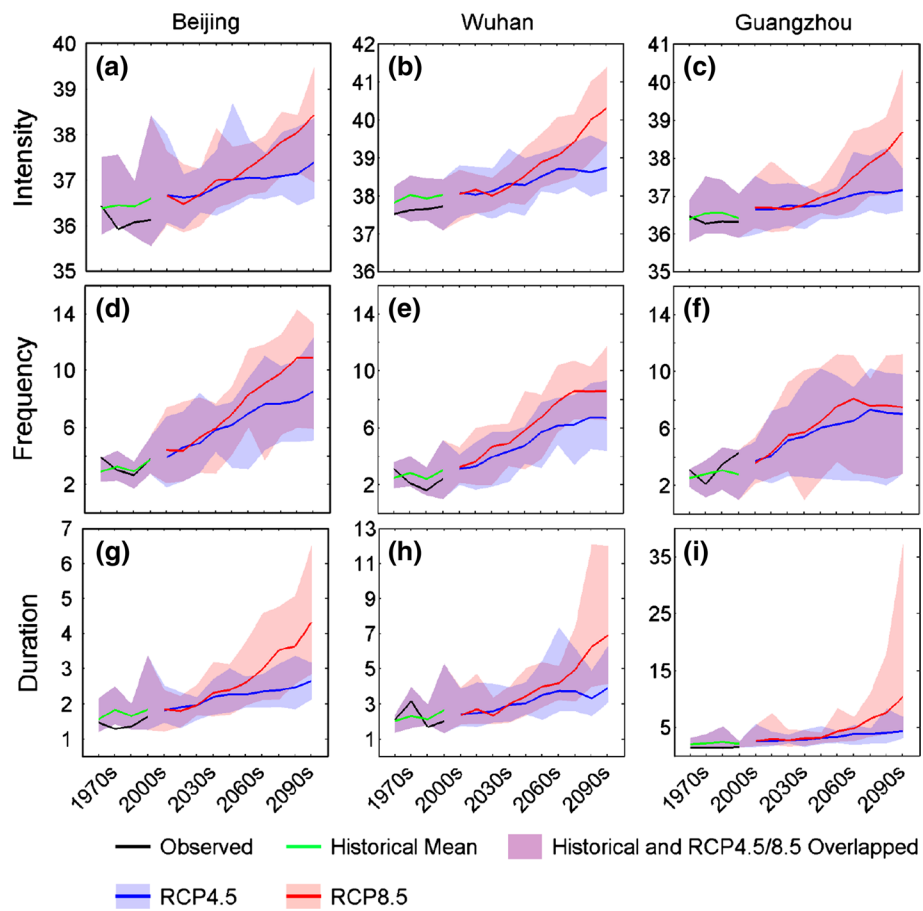
Secular trends in hot spell intensity, frequency, and duration for all GCMs in the historical experiment from 1960–2005 as estimated by the HSM are conducted. Ensemble means of these trends are not meaningful when taking the 0.05 significance level into consideration (if only trends significant at the 0.05 level are shown, as in Fig. 4d–f), as the p values are estimated by the HSM in each GCM individually. In addition, it is cumbersome to show the fitted trend results of all GCMs individually. Therefore, these figures are not shown. However, we can summarize the main

features. Generally, compared to the localized significant increasing trends in all three hot spell components in observations (Fig. 4d–f), it is found that significant increasing trends in hot spell intensity are localized in most GCMs, with deviations from observations, while the trends in hot spell frequency are more widespread in the GCMs. The GCMs with significant pattern correlations with observations can more or less capture the significant increasing trend in southeastern, western, and northeastern regions; very few GCMs can reproduce the exact location of significant decreasing trend in east-central China.

The ensemble mean of the hot spell intensity, frequency, and duration of 12 selected GCMs in the historical run in 1960–2005 is given in Fig. 5a–c. Meanwhile, differences in these hot spell components between the ensemble mean in the GCMs and the observations in the same period are shown in Fig. 5d–f. These differences are calculated by subtracting the observation values from the values in the GCM ensemble means. Note that the grid point data of the GCMs are interpolated into 549 gauge station locations, as mentioned above. Only one climatological mean value is obtained for each spatial point, so there is no need to discuss the statistical significance of the difference.

Figure 5a shows that the observed geographic pattern of hot spell intensity, with a low intensity center on the Tibetan Plateau and relatively high intensity in Southeast and Northwest China, can be basically reproduced by the GCMs. However, if no bias correction was applied to the GCM T_{\max} data, there would be large biases in the modeled hot spell intensity compared to observations. All GCMs underestimate the hot spell intensities in southwestern China, roughly over the Tibetan Plateau. But it is

Fig. 6 Ensemble mean hot spell intensity (a–c, °C), frequency (d–f, events/year), and duration (g–i, days) in Beijing (a, d, g), Wuhan (b, e, h), and Guangzhou (c, f, i) averaged decade by decade in the 1960s–2090s. Black lines represent observations, green lines represent the historical run, blue lines represent RCP4.5, and red lines represent RCP8.5. Blue shading represents the ensemble ranges of RCP4.5, red shading represents the ensemble ranges of RCP8.5, and purple shading represents the ensemble ranges of the historical run and the overlap regions of RCP4.5 and RCP8.5



also noteworthy that observations in this area are scarce, as shown in Fig. 1. With the bias correction mentioned above, differences between the ensemble mean hot spell intensity and observations is less than ± 1 °C. A maximum positive bias (ensemble mean larger than observations) is about 1 °C, appearing in a small region of Southwest China. Positive biases are found in most areas of China, while negative biases are found in the lower Yellow River Valley and Northeast China. The maximum negative bias is about -0.7 °C (Fig. 5d). Figure 5e, f suggest that climate models underestimate the hot spell frequency and overestimate the hot spell duration in southern regions of China. The maximum bias of the ensemble mean hot spell frequency in southern China is -1.4 event/year, while the maximum bias of ensemble mean hot spell duration in the same region is 1.7 days. These biases result in higher frequency (shorter duration) to the north and lower frequency (longer duration) to the south, as shown in Fig. 5b, c. That is to say, the observed mean geographic pattern of hot spell frequency and duration given in Fig. 4b, c cannot be fully captured by the climate models. Synoptic characters of local climate may exist in the geographic pattern of hot spell frequency and duration, which are hard to reproduce. Most of the GCMs present a meridionally varying pattern of high

frequency and short duration in the north, and the reverse in the south.

In the application of HSM to observations in China, we use three demonstration sites, Beijing, Wuhan, and Guangzhou, to show the fitting results. These stations are chosen to further demonstrate the hot spell characteristics estimated by HSM in CMIP5 simulations. The 12-member ensemble mean hot spell intensity, frequency, and duration at the three demonstration stations in each decade during 1960–2099 is given in Fig. 6. Black lines and green lines represent observations and ensemble means of the historical run in the 1960s–1990s, respectively. Generally, the ensemble means obtain values closer to observations in all three hot spell components compared to individual GCMs (purple shading in 1960s–1990s represents the ensemble range of the historical run), but the observed interdecadal (and interannual) variations are not well captured. Future projection in the RCP4.5 and RCP8.5 scenarios will be further discussed in the next subsection.

4.2 Future projections

In Fig. 6, blue lines represent RCP4.5, and red lines represent RCP8.5. Blue shading represents the ensemble range

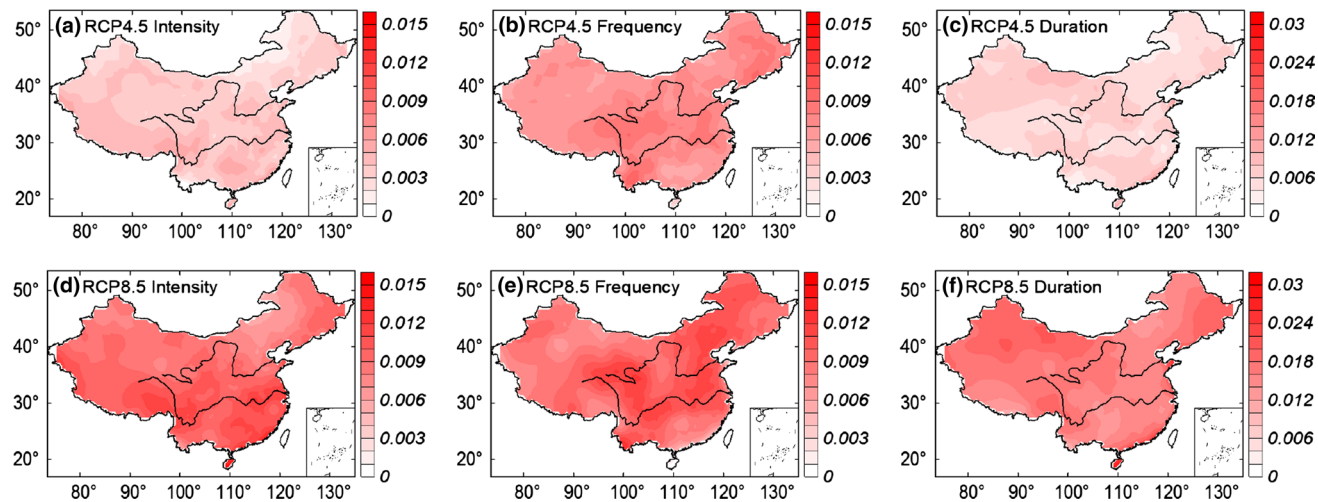


Fig. 7 Ensemble mean of estimated trends of hot spell intensity (**a** and **d**, °C/year), frequency (**b** and **e**, events/year), and duration (**c** and **f**, days/year) in RCP4.5 (**a–c**) and RCP8.5 (**d–f**) in 2006–2100. All

trends are simply estimated to be significant at the 0.05 level, as most of the p values in the GCMs are <0.05 in the future conditions

of RCP4.5, red shading represents the ensemble range of RCP8.5, and purple shading in the 2010s–2090s represents the overlap region of the RCP4.5 and RCP8.5 ensemble ranges. Monotonic increases in hot spell intensity, frequency, and duration are found at all three demonstration sites in future scenarios, with RCP8.5 larger than RCP4.5, as expected. In practice, Fig. 6 shows the values of hot spell components averaged decade by decade, but not the exponential increasing trends estimated by HSM, such as the solid lines in Fig. 3. The exponentially increasing lines fitted by HSM can be conducted in each GCM individually but may not be appropriate to show in an average form.

As mentioned above, the p values used to determine the significance levels of these trends are estimated in each individual GCM by the HSM and are not suitable for averaging in all GCMs. However, it is found that trends of hot spell components in all GCMs in the future scenarios are basically significant at the 0.05 level in all of the stations over China. Therefore, the ensemble mean trend values are simply estimated as significant at the 0.05 level at all sites. The 12-member ensemble hot spell trends in 2006–2100 estimated by the HSM in RCP4.5 and RCP8.5 are shown in Fig. 7. It is noteworthy that these trend values represent the magnitude of the parameter rate change per year. The hot spell components estimated by the HSM increase nonlinearly (e.g., exponentially in hot spell frequency) with these parameters. For hot spell intensity, the maximum exponential rate of increase is 0.007 °C/year in RCP4.5 (Fig. 7a) and 0.015 °C/year in RCP8.5 (Fig. 7d). For hot spell frequency, the maximum exponential rate of increase is 0.010 event/year in RCP4.5 (Fig. 7b) and 0.013 event/year in RCP8.5 (Fig. 7e). For hot spell duration, the maximum exponential rate of increase is 0.017 day/year in

Table 4 Same as Table 3 but for ensemble projection trends in 2006–2100 in RCP4.5 and RCP8.5

Hot Spell	RCPs	Beijing	Wuhan	Guangzhou
Intensity (°C/year)	RCP4.5	0.003	0.004	0.004
	RCP8.5	0.008	0.012	0.011
Frequency (events/year)	RCP4.5	0.008	0.008	0.006
	RCP8.5	0.011	0.011	0.007
Duration (days/year)	RCP4.5	0.005	0.004	0.008
	RCP8.5	0.015	0.016	0.018

p values are not given as they are estimated in each GCM individually. As most of the p values are <0.05 in the future conditions, all trends in this table are estimated to be significant at the 0.05 level

RCP4.5 (Fig. 7c) and 0.029 day/year in RCP8.5 (Fig. 7f). The exact values of the 12-member ensemble mean hot spell trends in the three demonstration sites in 2006–2100 estimated by the HSM in the two RCP scenarios are given in Table 4. At these stations, hot spell intensity increases by 0.003–0.012 °C/year, hot spell frequency increases by 0.006–0.011 event/year, and hot spell duration increases by 0.004–0.018 day/year, as estimated by the HSM in IPCC AR5 scenarios during 2006–2100.

Next, we project the averaged results for the last decade of the twenty-first century, i.e., the 2090s, to offer estimations for this particular time period under future conditions. These results are shown in Figs. 8 and 9 for all stations in China. Panels a–c are absolute values of estimated hot spell intensity, frequency, and duration, respectively, while panels d–f are the increased values compared to the ensemble mean in the historical run (see Fig. 5). The color scale is the same in RCP4.5 and RCP8.5 for hot spell intensity, that is, the same as in Figs. 8a and 9a, and

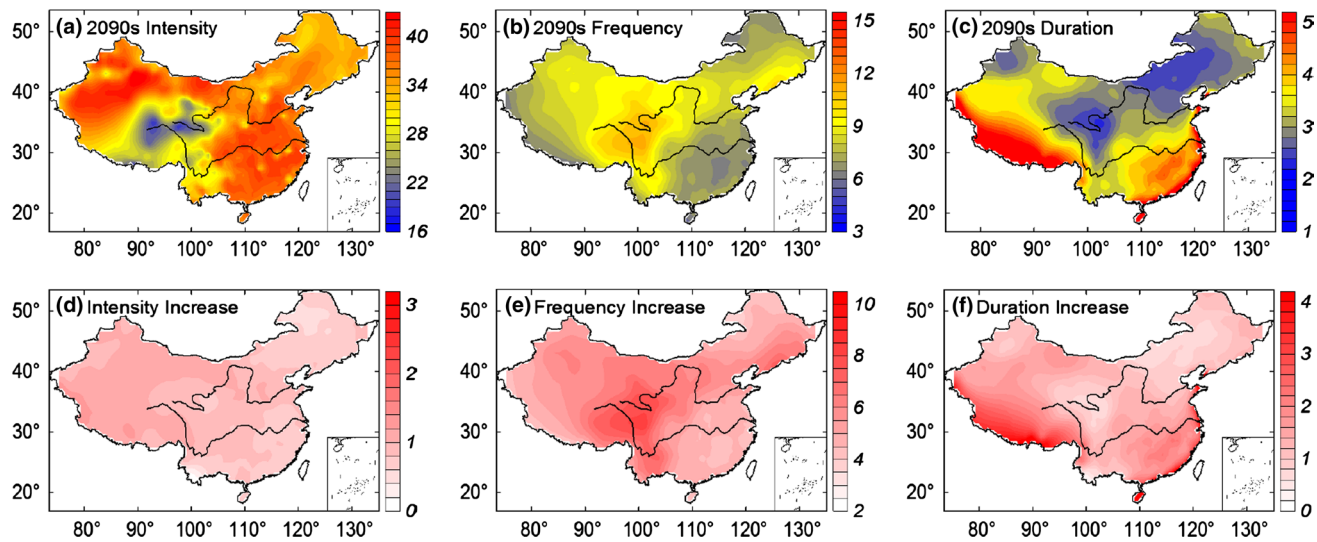


Fig. 8 Ensemble mean of estimated hot spell intensity (**a**, °C), frequency (**b**, events/year), and duration (**c**, days) in the 2090s in RCP4.5, and their increases from the historical ensemble mean (**d–f**)

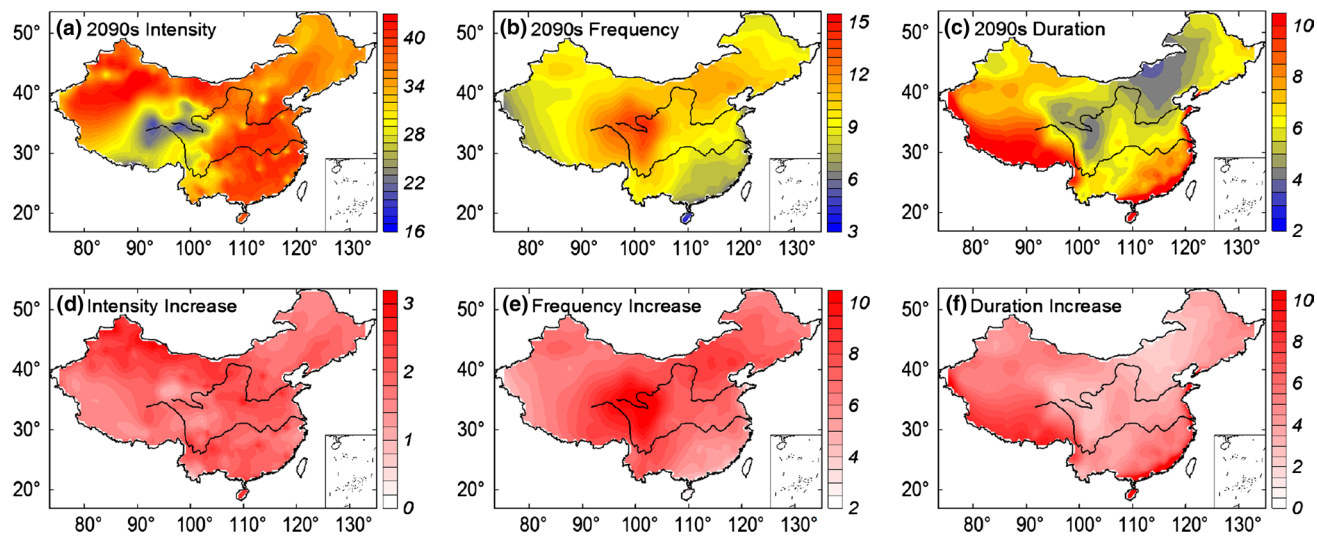


Fig. 9 Same as Fig. 8 but for RCP8.5

the same as in Figs. 8d and 9d. It is also the same for hot spell frequency. But the differences between RCP4.5 and RCP8.5 in hot spell duration are too large to keep the same color scale. The estimated hot spell intensity in China in the 2090s ranges from 18.8 to 44.9 °C in RCP4.5, with a maximum increase of 1.4 °C from the historical run (Fig. 8a, d). It ranges from 19.7 to 45.8 °C in RCP8.5, with a maximum increase of 3.1 °C from the historical run (Fig. 9a, d). The magnitude of increase in the hot spell intensity is comparable to the increase in mean temperature in IPCC AR5 scenarios. Both hot spell frequency and duration show a remarkable increase. Estimated hot

spell frequency (events/year) ranges from 5.0 to 11.3 in RCP4.5, with a maximum increase of 8.4 from the historical run (Fig. 8b, e). It ranges from 3.6 to 14.3 in RCP8.5, with a maximum increase of 11.2 from the historical run (Fig. 9b, e). The increase in the duration is stronger than that in the frequency in the eastern coastal and southern regions, where increases in the hot spell duration from the historical run are more than 10 days (Figs. 8c, f, 9c, f). Moreover, along the Yellow River valley, especially around its upper reaches, hot spells have higher frequencies and shorter durations compared to those of other regions in the 2090s.

Table 5 Estimated ensemble mean hot spell intensity, frequency, and duration in Beijing, Wuhan, and Guangzhou during 1960–2005 (historical run) and the 2090 s (RCP4.5 and RCP8.5)

Hot spell	Experiment (Period)	Beijing	Wuhan	Guangzhou
Intensity (°C)	Historical (1960–2005)	36.5	38.0	36.5
	RCP4.5 (2090s)	37.4	38.8	37.1
	RCP8.5 (2090s)	38.3	39.9	38.5
Frequency (events)	Historical (1960–2005)	2.9	2.1	2.3
	RCP4.5 (2090s)	8.4	6.7	6.9
	RCP8.5 (2090s)	10.8	8.6	7.4
Duration (days)	Historical (1960–2005)	1.7	2.3	2.3
	RCP4.5 (2090s)	2.7	3.9	4.4
	RCP8.5 (2090s)	4.3	6.9	10.4

Numerical details for the three illustrative sites in the 2090s are given in Table 5. Results of the historical experiments (12-member ensemble in 1960–2005) are also listed in the table for comparison. All numbers in Table 5 are given in absolute form, that is, without subtracting the historical values. The increases in intensity are <1 °C with RCP4.5, and about 2 °C with RCP8.5 for all three sites. Both hot spell frequency and duration show a remarkable increase at these stations, as is evident in Fig. 6. Finally, if we calculate the total number of hot days from Table 5, that is, hot spell frequency multiplied by duration, we find that there is a dramatic increase in this extreme event. Days with T_{\max} above the present threshold would increase from 4.9 (historical) to 46.4 per summer in the 2090s in Beijing with RCP8.5, for example.

5 Conclusions and discussion

Hot spells and are multifaceted forms of extreme climatic events. In the statistical study of these climatic extremes, one challenge is how to model the temporal clustering of temperatures at high levels. In this study, we use the 95th percentile of local temperature to define hot spells in China and investigate these hot spells using the statistical theory of extreme values. The HSM models the hot spell intensity, frequency, and duration with the GP, Poisson, and geometric distributions, respectively. Results from Beijing, Wuhan, and Guangzhou suggest that the HSM can realistically model hot spells. We then apply the HSM to all gauge stations in China to obtain spatial patterns and temporal trends of hot spells. More importantly, trends in hot spell characteristics can be obtained by allowing parametric changes in time for these extreme event distributions, which is the

most common approach for dealing with nonstationarity and has shown practical utility in assessing long-term changes in climatic extreme events.

Statistics of observed hot extremes are needed to compare with climate model simulations, and hence to detect trends in future projections (e.g., Meehl and Tebaldi 2004). We assess the simulation of the HSM in CMIP5, a newly available state-of-the-art GCM ensemble, to perform this step. With the 95th percentile threshold as the definition of hot spells, the total number of hot days, that is, the frequency of hot spells multiplied by their length, is fitted. Therefore, synoptic characters of local climate may be hidden in the geographic distribution of hot spell frequency and duration (observations shown in Fig. 4b, c). For instance, in the lower Yangtze River valley, hot spells persist longer and appear with lower frequency compared to those of other areas. However, these geographic patterns are difficult to reproduce in GCMs.

Ensemble projections of hot spells to upcoming decades of the twenty-first century are also conducted using “good performance” climate models from the assessment. With the focus on this objective of future projection, the main criterion of “good performance” is simply that the major features of the geographic pattern in secular trends in observations can be reproduced in the historical simulations. These major features are objectively assessed as significant pattern correlations with observations in all three hot spell characteristics. A total of 30 GCMs are discussed in detail, and two RCP scenarios are involved. Scenario RCP8.5, with an emphasis on radiative forcing conditions, is found to provide the most rapidly increasing trend in hot extremes (Sillmann et al. 2013b). In general, this study provides only a first-order evaluation of the performance of CMIP5 models in terms of hot spells in China.

Other challenges in the statistical modeling of hot extremes include whether multivariate extreme value theory can be used to model climate variables that can contribute to hot spells and heat waves, such as maximum and minimum temperature, dew point or humidity, wind speed, and cloud cover. Generally speaking, there is a need for improvement in the statistical modeling of heat waves and other meteorological extremes. These variables that can affect changes in temperature extremes should also be taken into account in the assessment.

Hot spells and heat waves usually coincide with specific atmospheric circulation patterns. Recurrences of these circulation patterns in climate models are important to the simulation of climatic extreme events and future projections. This study focuses mainly on the simulation of summer temperatures and extremes. Investigations of simulations of large-scale circulations associated with temperature extremes are needed in future studies. Furthermore, hot extremes can be systematically affected by changes

in land use and land cover (e.g., Zhang and Li 2009; Zhao and Pitman 2002). The IPCC AR4 (IPCC 2007) has pointed out that in middle- and high-latitude continental areas, the observed decadal trends of extreme temperatures can probably be attributed to human activities. China has experienced rapid urbanization since the 1970s, and some previous studies have focused on the impact of land use and urbanization on extreme hot events (Hu et al. 2010; Jones et al. 2008; Ren et al. 2008; Zhang and Wu 2011). However, to what extent urbanization accounts for surface warming is still hard to clarify. GCM assessment may be further complemented by more detail on these issues.

Acknowledgments This study is supported by the National Nature Science Foundation of China Grant 41175079 and 41376025, the Macao Meteorological and Geophysical Bureau (SMG) Project 9231048, and the Strategic Priority Research Program of the Chinese Academy of Sciences Grant XDA11010403. Y. Li was supported by CSIRO Climate Adaptation Flagship. This work was initiated when the first author visited CSIRO in his PhD study leave during 1 October–30 November 2011, supported by Chow Yei Ching School of Graduate Studies, City University of Hong Kong.

References

- Barnett TP, Schlesinger ME (1987) Detecting changes in global climate induced by greenhouse gases. *J Geophys Res Atmos* 92:14772–14780
- Brown BG, Katz RW (1995) Regional analysis of temperature extremes: spatial analog for climate change? *J Clim* 8:108–119
- Brown SJ, Caesar J, Ferro CAT (2008) Global changes in extreme daily temperature since 1950. *J Geophys Res Atmos* 113:D05115. doi:[10.1029/2006JD008091](https://doi.org/10.1029/2006JD008091)
- Coles S (2001) An introduction to statistical modeling of extreme values. Springer, London
- Ding T, Qian WH (2011) Geographical patterns and temporal variations of regional dry and wet heatwave events in China during 1960–2008. *Adv Atmos Sci* 28(2):322–337
- Ding Y, Sun Y, Wang Z, Zhu Y, Song Y (2009) Inter-decadal variation of the summer precipitation in China and its association with decreasing Asian summer monsoon. Part II: possible causes. *Int J Climatol* 29:1926–1944
- Easterling DR, Meehl GA, Parmesan C et al (2000) Climate extremes: observations, modeling, and impacts. *Science* 289:2068–2074
- Fischer T, Menz C, Su B, Scholten T (2013) Simulated and projected climate extremes in the Zhujiang River Basin, South China, using the regional climate model COSMO-CLM. *Int J Climatol*. doi:[10.1002/joc.3643](https://doi.org/10.1002/joc.3643)
- Furrer EM, Katz RW (2008) Improving the simulation of extreme precipitation events by stochastic weather generators. *Water Resour Res* 44:W12439. doi:[10.1029/2008WR007316](https://doi.org/10.1029/2008WR007316)
- Furrer EM, Katz RW, Walter MD, Furrer R (2010) Statistical modeling of hot spells and heat waves. *Clim Res* 43:191–205
- Gong D, Pan Y, Wang J (2004) Changes in extreme daily mean temperatures in summer in eastern China during 1955–2000. *Theor Appl Climatol* 77:25–37
- Gumbel EJ (1958) Statistics of extremes. Columbia University Press, New York
- Houghton JT, Ding Y, Griggs DJ, Noguer M, van der Linden PJ, Dai X, Maskell K, Johnson CA (eds) (2001) IPCC, 2001: Climate change 2001: the physical science basis. Contribution of working group I to the third assessment report of the intergovernmental panel on climate change. Cambridge University Press, Cambridge, UK and New York, NY, USA
- Hu Y, Dong W, He Y (2010) Impact of land surface forcings on mean and extreme temperature in eastern China. *J Geophys Res* 115:D19117. doi:[10.1029/2009JD013368](https://doi.org/10.1029/2009JD013368)
- Jones P, Horton E, Folland C, Hulme M, Parker D, Basnett T (1999) The use of indices to identify changes in climatic extremes. *Clim Change* 42:131–149
- Jones P, Lister D, Li Q (2008) Urbanization effects in large-scale temperature records, with an emphasis on China. *J Geophys Res* 113:D16122. doi:[10.1029/2008JD009916](https://doi.org/10.1029/2008JD009916)
- Jones GS, Stott PA, Christidis N (2013) Attribution of observed historical near-surface temperature variations to anthropogenic and natural causes using CMIP5 simulations. *J Geophys Res Atmos* 118:4001–4024
- Karl TR, Nicholls N, Ghazi A (1999) CLIVAR/GCOS/WMO workshop on indices and indicators for climate extremes. *Clim Change* 42:3–7
- Katz RW, Parlange MB, Naveau P (2002) Statistics of extremes in hydrology. *Adv Water Resour* 25:1287–1304
- Katz RW, Brush GS, Parlange MB (2005) Statistics of extremes: modeling ecological disturbances. *Ecology* 86:1124–1134
- Knutti R, Sedlacek J (2012) Robustness and uncertainties in the new CMIP5 coordinated climate model projections. *Nat Clim Change* 3:369–373
- Legates DR, Davis RE (1997) The continuing search for an anthropogenic climate change signal: limitations of correlation based approaches. *Geophys Res Lett* 18:2319–2322
- Li Z, Yan ZW (2009) Homogenized daily mean/maximum/minimum temperature series for China from 1960–2008. *Atmos Oceanic Sci Lett* 2:237–243
- Li Z, Yan ZW (2010) Application of multiple analysis of series for homogenization to Beijing daily temperature series (1960–2006). *Adv Atmos Sci* 27(4):777–787. doi:[10.1007/s00376-009-9052-0](https://doi.org/10.1007/s00376-009-9052-0)
- Li Y, Cai W, Campbell EP (2005) Statistical modeling of extreme rainfall in southwest Western Australia. *J Clim* 18:852–863
- Li L, Wang B, Zhou T (2007) Contributions of natural and anthropogenic forcings to the summer cooling over eastern China: an AGCM study. *Geophys Res Lett* 34:L18807. doi:[10.1029/2007GL030541](https://doi.org/10.1029/2007GL030541)
- Li H, Dai A, Zhou T, Lu J (2010) Responses of East Asian summer monsoon to historical SST and atmospheric forcing during 1950–2000. *Clim Dyn* 34:501–514
- Meehl GA, Tebaldi C (2004) More intense, more frequent, and longer lasting heat waves in the 21st century. *Science* 305:994–997
- Meehl GA et al (2000) An introduction to trends in extreme weather and climate events: Observations, socioeconomic impacts, terrestrial ecological impacts, and model projections. *Bull Am Meteorol Soc* 81:413–416
- Menon S, Hansen J, Najarenko L, Luo Y (2002) Climate effects of black carbon aerosols in China and India. *Science* 297:2250–2252
- Nogaj M, Yiou P, Parey S, Malek F, Naveau P (2006) Amplitude and frequency of temperature extremes over the North Atlantic region. *Geophys Res Lett* 33:L10801. doi:[10.1029/2005GL024251](https://doi.org/10.1029/2005GL024251)
- Parmesan C, Root TL, Willig MR (2000) Impacts of extreme weather and climate on terrestrial biota. *Bull Am Meteorol Soc* 81:443–450
- Qian W, Lin X (2004) Regional trends in recent temperature indices in China. *Clim Res* 27:119–134
- Qian C, Zhou T (2014) Multidecadal variability of North China aridity and its relationship to PDO during 1900–2010. *J Clim* 27(3):1210–1222
- Qian C, Yan ZW, Wu Z, Fu CB, Tu K (2011a) Trends in temperature extremes in association with weather-intraseasonal fluctuations in eastern China. *Adv Atmos Sci* 28(2):297–309

- Qian C, Wu Z, Fu C, Wang D (2011b) On changing El Niño: a view from time-varying annual cycle, interannual variability and mean state. *J Clim* 24(24):6486–6500
- Ren GY, Chu ZY, Chen ZH, Ren YY (2007) Implications of temporal change in urban heat island intensity observed at Beijing and Wuhan stations. *Geophys Res Lett* 34:L05711. doi:[10.1029/2006GL027927](https://doi.org/10.1029/2006GL027927)
- Ren GY, Zhou YQ, Chu ZY, Zhou JX, Zhang AY, Guo J, Liu XF (2008) Urbanization effects on observed surface air temperature trends in north China. *J Clim* 21:1333–1348
- Robinson PJ (2001) On the definition of a heat wave. *J Appl Meteorol* 40:762–775
- Santer BD, Wigley TML, Jones PD (1993) Correlation methods in fingerprint detection studies. *Clim Dyn* 8:265–276
- Sillmann J, Kharin VV, Zhang X, Zwiers FW, Bronaugh D (2013a) Climate extremes indices in the CMIP5 multimodel ensemble: Part 1. Model evaluation in the present climate. *J Geophys Res Atmos* 118:1716–1733
- Sillmann J, Kharin VV, Zwiers FW, Zhang X, Bronaugh D (2013b) Climate extremes indices in the CMIP5 multimodel ensemble: part 2. Future climate projections. *J Geophys Res Atmos* 118:2473–2493
- Smith RL (1989) Extreme value analysis of environmental time series: An application to trend detection in ground-level ozone (with discussion). *Stat Sci* 4:367–393
- Solomon S, Qin D, Manning M, Chen Z, Marquis M, Averyt KB, Tignor M, Miller HL (eds) (2007) IPCC, 2007: Climate change 2007: the physical science basis. Contribution of working group I to the fourth assessment report of the intergovernmental panel on climate change. Cambridge University Press, Cambridge, UK and New York, NY, USA
- Stocker TF, Qin D, Plattner GK, Tignor M, Allen SK, Boschung J, Nauels A, Xia Y, Bex V, Midgley PM (eds) IPCC, 2013: climate change 2013: the physical science basis. Contribution of working group I to the fifth assessment report of the intergovernmental panel on climate change. Cambridge University Press, Cambridge, UK and New York, NY, USA
- Su BD, Jiang T, Jin WB (2006) Recent trends in observed temperature and precipitation extremes in the Yangtze River basin, China. *Theor Appl Climatol* 83(1–4):139–151
- Tao S, Wei J (2006) The westward, northward advance of the subtropical high over the west Pacific in summer. *J Appl Meteorol Sci* 17(5):513–525 (in Chinese)
- Taylor KE, Stouffer RJ, Meehl GA (2012) An overview of CMIP5 and the experiment design. *Bull Am Meteorol Soc* 93:485–498
- Todorovic P, Zelenhasic E (1970) A stochastic model for flood analysis. *Water Resour Res* 6:1641–1648
- Ueda H, Iwai A, Kuwako K, Hori ME (2006) Impact of anthropogenic forcing on the Asian summer monsoon as simulated by eight GCMs. *Geophys Res Lett* 33:L06703. doi:[10.1029/2005GL025336](https://doi.org/10.1029/2005GL025336)
- Wang W, Zhou W, Wang X, Fong SK, Leong KC (2013a) Summer high temperature extremes in Southeast China associated with the East Asian jet stream and circumglobal teleconnection. *J Geophys Res Atmos* 118. doi:[10.1002/jgrd.50633](https://doi.org/10.1002/jgrd.50633)
- Wang X, Zhou W, Wang D, Wang C (2013b) The impacts of the summer Asian jet stream biases on surface air temperature in mid-eastern China in IPCC AR4 models. *Int J Climatol* 33:265–276. doi:[10.1002/joc.3419](https://doi.org/10.1002/joc.3419)
- Wang W, Zhou W, Chen D (2014) Summer high temperature extremes in Southeast China: bonding with the El Niño-Southern Oscillation and East Asian summer monsoon coupled system. *J Clim* 27:4122–4138
- Xu Q (2001) Abrupt change of the mid-summer climate in central east China by the influence of atmospheric pollution. *Atmos Environ* 35:5029–5040
- Yan Z, Yang C, Jones PD (2001) Influence of inhomogeneity on the estimation of mean and extreme temperature trends in Beijing and Shanghai. *Adv Atmos Sci* 18:309–322
- Yan Z, Jones PD, Davies TD et al (2002) Trends of extreme temperatures in Europe and China based on daily observations. *Clim Change* 53:355–392
- Yan Z, Li Z, Li Q, Jones P (2010) Effects of site change and urbanization in the Beijing temperature series 1977–2006. *Int J Climatol* 30:1226–1234
- Yan Z, Xia J, Qian C et al (2011) Changes in seasonal cycle and extremes in China during the period 1960–2008. *Adv Atmos Sci* 28:269–283
- You Q, Kang S, Aguilar E, Yan Y (2008) Changes in daily climate extremes in the eastern and central Tibetan Plateau during 1961–2005. *J Geophys Res* 113:D07101. doi:[10.1029/2007JD009389](https://doi.org/10.1029/2007JD009389)
- Yu R, Zhou T (2007) Seasonality and three-dimensional structure of the interdecadal change in East Asian monsoon. *J Clim* 20:5344–5355
- Yu R, Wang B, Zhou T (2004) Tropospheric cooling and summer monsoon weakening trend over East Asia. *Geophys Res Lett* 31:L22212. doi:[10.1029/2004GL021270](https://doi.org/10.1029/2004GL021270)
- Zhai P, Pan XH (2003) Trends in temperature extremes during 1951–1999 in China. *Geophys Res Lett* 30(17):1913–1916
- Zhang H, Li Y (2009) Potential impacts of land-use on climate variability and extremes. *Adv Atmos Sci* 26:840–854
- Zhang JY, Wu LY (2011) Land-atmosphere coupling amplifies hot extremes over China. *Chin Sci Bull* 56:3328–3332
- Zhang XB, Zwiers FW, Li GL (2004) Monte Carlo experiments on the detection of trends in extreme values. *J Clim* 17:1945–1952
- Zhang Q, Xu C-Y, Zhang Z, Ren G, Chen YD (2008) Climate change or variability? The case of Yellow River as indicated by extreme maximum and minimum air temperature during 1960–2004. *Theor Appl Climatol* 93:35–43
- Zhao M, Pitman AJ (2002) The impact of land cover change and increasing carbon dioxide on the extreme and frequency of maximum temperature and convective precipitation. *Geophys Res Lett* 29:1078. doi:[10.1029/2001GL013476](https://doi.org/10.1029/2001GL013476)
- Zhou W, Li CY, Chan JCL (2006) The interdecadal variations of the summer monsoon rainfall over South China. *Meteorol Atmos Phys*. doi:[10.1007/S00703-006-018-9](https://doi.org/10.1007/S00703-006-018-9)